Super-Twisting Control with Quaternion Feedback for a 3-DOF Inertial Stabilization Platform

Matheus F. Reis, João C. Monteiro, Ramon R. Costa

***Abstract*— The majority of works in line of sight (LOS) stabilization and tracking using inertially stabilized platforms (ISP) apply simple linear controllers to achieve the required performance. Commonly, linear models such as a double integrator with an inertia gain are employed to describe the relationship between torque and position of the ISP joints. However, these techniques do not provide ideal disturbance rejection or finite-time convergence, which are desired characteristics for these type of systems in the context of high-accuracy applications.**

In this work, we propose a novel Sliding Mode Control (SMC) strategy for both stabilization and orientation tracking for a 3-DOF ISP. Full state feedback and output feedback cases are considered. In the latter case, a High-Order Sliding Mode observer (HOSMO) is proposed for the estimation of the ISP joint velocities. In each case, two Super Twisting Controllers (STC) are employed in a cascade topology. The inner controller ideally rejects the *dynamic* disturbances acting on the ISP joints, reducing the system to an ideal double integrator. The outer controller ensures orientation tracking in quaternion space, ideally rejecting all remaining kinematic disturbances.

Numerical simulations show the efficiency and performance of the proposed controller and observer.

I. Introduction

Line-of-sight (LOS) stabilization is a challenging problem. Inertially stabilized platforms (ISP) are widely used for payload stabilization and tracking applications, when a sensor must accurately point to a target in a dynamic environment. Some examples are cameras for aerial surveying and entertainment industry [1], long-range sensors on vehicles [2], military applications [3] and thermal cameras for oil spill detection [4].

ISPs are gimbaled structures, usually mounted on a mobile base (vehicle), driven by motors equipped with encoders/tachometers and a payload fixed on the last gimbal. Gyroscopes or inertial navigation systems (INS) are employed in the control loop by either measuring the vehicle motion (*indirect stabilization*) or directly measuring the payload motion (*direct stabilization*) [5]. The latter is usually recommended for precision pointing applications, since the sensor location is appropriate for capturing other effects that can impact the measured angular rates, such as structure flexibility, resolvers, tachometer and/or encoder accuracy and processor sampling rate [5]. A possible drawback of this method is the larger size of the gimbals required to support the larger payload induced by the weight of the sensors in the inner gimbal. This drawback is usually absent in the indirect method, but since the disturbances are not measured in the LOS coordinate frame, the control performance can be degraded.

The authors are with the Electrical Engineering Department of COPPE/UFRJ, Rio de Janeiro, Brazil matheus.ferreira.reis@gmail.com, {jcmonteiro, ramon}@coep.ufrj.br

Simple dynamic models describing this type of system are common in the literature. Usually, the joints are considered as decoupled and a double integrator model with an inertia gain relates the joint torque and position. Unmodeled dynamics, such as the vehicle motion and cross-coupling effects, are treated as disturbances to be rejected.

The typical control topology is P-PI control. Usually, the inner PI velocity loop has a high bandwidth to stabilize the payload and attenuate the torque disturbances. The outer proportional orientation loop operates at a lower bandwidth and minimizes the pointing error [6], [7], [8]. However, in *high accuracy* and/or *fast dynamics* applications, unmodeled effects may add significant torque contributions, and simple linear controllers may not suffice for the required level of performance.

Some works have tackled the problem of LOS control for ISPs in a more detailed way. In [9], the effects of kinematic coupling of the base and gimbal imbalance are analyzed for a 2-DOF ISP, while [10] proposes a self-tunning PID-type fuzzy controller as an alternative to PID control used in the ISP internal stabilization loop. Recently, [11] used the unit quaternion formalism for attitude stabilization, proposing a control method based in feedback linearization that takes partial advantage of the ISP Lagrangian model. In [12], it is shown that even in the presence of large parameter uncertainties, a computed-torque plus PID (CTPID) controller guarantees satisfactory performance.

Modern techniques using Sliding Mode Control (SMC) are being applied for ISP stabilization and tracking. Their attractive characteristics include: (i) exact rejection of bounded matched disturbances; (ii) finite-time convergence and (iii) ease of implementation. For example, in [13], a Non-singular Terminal Sliding Mode controller [14] is used to achieve finite-time stabilization of an ISP in the presence of bounded matched disturbances affecting its electromechanical system. To avoid measuring the system state, High-Order Sliding Mode (HOSM) observers are employed.

In this work, a novel cascade control strategy based on the super-twisting algorithm (STA) is used to tackle the problem of ISP stabilization and tracking. Two cases are considered: (i) full state feedback, where the ISP joint angles and velocities are measured and (ii) output feedback, where

the ISP joint velocities are estimated using an observer based on higher-order sliding mode (HOSM) theory. Stability analysis is performed, and numerical simulations show the efficiency and performance of the proposed control schemes.

II. ISP Modeling

In this section, a procedure for deriving the kinematic and dynamic models of an ISP installed on a moving base is presented.

A. Notations and Conventions

Let $\mathbb{N} = \{0, 1, 2, \dots\}$ denote the set of *natural numbers*. Unless otherwise stated, $i, j, k \in \mathbb{N} \cup \{s, c\}$. Define:

- $\mathbf{E}_w$: world frame, arbitrarily located;
- $\mathbf{E}_{\bar{i}}$: frame fixed on body i with origin on its center of gravity (CG) ($i \in \mathbb{N}_0$);
- $\mathbf{E}_i$: fixed on body i with origin on joint i axis ($i \in \mathbb{N}_0$);
- $\mathbf{E}_c$: camera frame, fixed on the last link;
- $x_i^k, y_i^k, z_i^k \in \mathbb{R}^3$: $\mathbf{E}_i$ canonical unit vectors, written in $\mathbf{E}_k$;
- $p_{ij}^k \in \mathbb{R}^3$: position vector from the origin of frame $\mathbf{E}_i$ to the origin of $\mathbf{E}_j$, represented in $\mathbf{E}_k$;
- $v_{ij}^k \in \mathbb{R}^3$: linear velocity from $\mathbf{E}_i$ to $\mathbf{E}_j$, written in $\mathbf{E}_k$;
- $\omega_{ij}^k \in \mathbb{R}^3$: angular velocity from $\mathbf{E}_i$ to $\mathbf{E}_j$, written in $\mathbf{E}_k$;
- $h_i^k \in \mathbb{R}^3$: unit vector defining the rotation axis of joint i, represented in $\mathbf{E}_k$ ($i = 1, 2, ...$);
- $m_i \in \mathbb{R}$, $I_i^i \in \mathbb{R}^{3\times3}$: mass and inertia tensor of body i represented in $\mathbf{E}_i$ ($i \in \mathbb{N}$);
- $\mathbf{S}(v) : \mathbb{R}^3 \mapsto \mathrm{so}(3)$ cross product operator;
- $\lfloor v \rceil^\alpha$: $\mathbb{R}^n \to \mathbb{R}^n$, where its elements are given by $\|v_i\|^\alpha \, sgn(v_i)$, with $v_i \in \mathbb{R}$ being the elements of $v \in \mathbb{R}^n$ and $\alpha \in \mathbb{R}$;
- $\mathbf{I}_n \in \mathbb{R}^{n\times n}$: identity matrix of dimension n.

Let body 0 be the moving base and bodies $1, 2, 3$ be the ISP gimbals. Also, if a superscript is omitted, the vector is written in world frame $\mathbf{E}_w$ coordinates.

B. Quaternion-Based Kinematics

Let $R \in SO(3)$ be a *rotation matrix* describing the rotation from an arbitrary frame to another. Then, R is a diffeomorphism with respect to the projective space $\mathbb{RP}^3 = \left\{ \|v\|^2 \leq \pi \mid v \in \mathbb{R}^3 \right\}$. Therefore, each point $v \in \mathbb{RP}^3$ is a 4-parameter representation for $SO(3)$ called the *angle-axis*, where the unitary vector on the direction of v represents the rotation axis and $\|v\|$ represents the corresponding rotation angle around that axis.

Remark 1. *Note that $\mathbb{RP}^3$ covers $SO(3)$ twice, since any point on it actually represents the same rotation than the opposite point of the sphere.*

This representation can be expressed by $v = \{\theta, n\}$, where $\theta \in \mathbb{R}$ is the angle of rotation around the unit axis vector $n \in \mathbb{R}^3, \|n\| = 1$. Another non-minimal representation is the *unit quaternion*. The set of *quaternions* $\mathbb{H}$ is defined by:

$$\begin{aligned} &\mathbb{H} := \{\eta + i\epsilon_1 + j\epsilon_2 + k\epsilon_3 \mid \eta, \epsilon_1, \epsilon_2, \epsilon_3 \in \mathbb{R}\} \,, \\ &i^2 = j^2 = k^2 = ijk = -1 \,. \end{aligned} \tag{1}$$

A quaternion $Q \in \mathbb{H}$ can also be represented as the pair $Q := \{\eta, \epsilon\}$, where $\eta = \mathsf{Re}(Q) \in \mathbb{R}$ represents the *real* part of the quaternion and $\epsilon = \mathsf{Im}(Q) = [\ \epsilon_1 \ \ \epsilon_2 \ \ \epsilon_3\ ]^\mathsf{T} \in \mathbb{R}^3$ represents the vector part. The quaternion *conjugate* is given by $Q^* = \{\eta, -\epsilon\}$. One can also represent the quaternion in fully vector form by the notation $\bar{Q} = [\ \eta \ \ \epsilon_1 \ \ \epsilon_2 \ \ \epsilon_3\ ]^\mathsf{T} \in \mathbb{R}^4$.

Quaternions also form an algebraic *group* with respect to *multiplication*. Given two quaternions $Q_1 = \{\eta_1, \epsilon_1\}$ and $Q_2 = \{\eta_2, \epsilon_2\}$, their multiplication follows the rules established by definition (1), which results in:

$$Q_1 \cdot Q_2 = \{\eta_1\eta_2 - \epsilon_1^\mathsf{T}\epsilon_2,\ \eta_1\epsilon_2 + \eta_2\epsilon_1 + \epsilon_1 \times \epsilon_2\} \,. \tag{2}$$

Quaternion multiplication can also be performed as a linear transformation in $\mathbb{R}^4$, by:

$$\overline{Q_1 \cdot Q_2} = \mathbf{H}_+(Q_1)\, \bar{Q}_2 \,, \tag{3}$$

$$= \mathbf{H}_-(Q_2)\, \bar{Q}_1 \,, \tag{4}$$

where $\mathbf{H}_+$, $\mathbf{H}_-$ are *Hamilton operators* defined by:

$$\mathbf{H}_+(Q) = \left[\ \overline{Q} \quad \mathbf{h}_+(Q)\ \right], \quad \mathbf{h}_+(Q) = \begin{bmatrix} -\epsilon^\mathsf{T} \\ \eta\,\mathbf{I}_3 + \widehat{\epsilon} \end{bmatrix} \tag{5}$$

$$\mathbf{H}_-(Q) = \left[\ \overline{Q} \quad \mathbf{h}_-(Q)\ \right], \quad \mathbf{h}_-(Q) = \begin{bmatrix} -\epsilon^\mathsf{T} \\ \eta\,\mathbf{I}_3 - \widehat{\epsilon} \end{bmatrix} \tag{6}$$

The square of the quaternion *norm* is defined as the *scalar*

$$\|Q\|^2 = Q \cdot Q^* = \{\eta^2 + \epsilon^\mathsf{T}\epsilon, 0\} \,, \tag{7}$$

and its *inverse* is the quaternion Q^{-1} such that $Q \circ Q^{-1} = \{1, 0\}$, the *unitary* quaternion.

The set of *unit quaternions* $\mathbb{H}^* = \{Q \in \mathbb{R} : \|Q\| = 1\}$ can be used as a parametrization for orientation in the following way. For an element $p = \{\theta, n\} \in \mathbb{RP}$, define:

$$Q = \left\{ cos\left(\frac{\theta}{2}\right), sin\left(\frac{\theta}{2}\right) n \right\} \in \mathbb{H}^* \,. \tag{8}$$

The inverse of an unit quaternion is given by $Q^{-1} = Q^*$, which according to (8), corresponds to the opposite rotation due to negative direction of the rotation axis n.

Let $r_0, r_1, ..., r_n \in \mathbb{H}^*$ be the n absolute rotations between frames $\mathbf{E}_0, \mathbf{E}_1, ..., \mathbf{E}_n$ and the world frame $\mathbf{E}_w$, and $r_{i+1}^i \in \mathbb{H}^*$ ($i = 1, 2, ..., n-1$) represent the rotations from frame $\mathbf{E}_i$ to $\mathbf{E}_{i+1}$. Since the unit quaternions form a group with respect to multiplication, then

$$r_n = r_1 \cdot r_2^1 \cdot ... \cdot r_n^{n-1} \in \mathbb{H}^* \,. \tag{9}$$

Now, define the set of *pure* quaternions $\mathbb{H}_p = \{v \in \mathbb{H} : \mathsf{Re}(v) = 0\}$. Note that any vector from $\mathbb{R}_3$ can be represented as the vector part of a corresponding element $v \in \mathbb{H}_p$. Let v^i and $v^j \in \mathbb{H}_p$ be representations for a vector $\vec{v}$ in frames

$\mathbf{E}_i$ and $\mathbf{E}_j$, respectively, and r_j^i represents the rotation from $\mathbf{E}_i$ to $\mathbf{E}_j$, with unitary axis $n_j^i \in \mathbb{R}^3$ and rotation angle θ_{ij}. Then, the following relation holds:

$$v^i = (r_j^i) \cdot v^j \cdot (r_j^i)^* = Ad_{r_j^i}\left[v^j\right] , \tag{10}$$

where $Ad_{r_j^i}[*]$ is the adjoint *operator*. Note that, in vector algebra, $Ad_{r_j^i}$ represents the corresponding rotation matrix $R_{ij} \in SO(3)$ associated to the unit quaternion $r_j^i \in \mathbb{H}^*$. In terms of the components of r_j^i, this matrix is given by

$$R_{ij} = n_j^i (n_j^i)^\mathsf{T} + s_{ij}\, \mathbf{S}(n_j^i) + c_{ij}\, (\mathbf{I}_3 - n_j^i (n_j^i)^\mathsf{T}) , \tag{11}$$

where s_{ij} and c_{ij} are the sine and cosine functions of θ_{ij}. The rotation matrix corresponding to an absolute rotation $r_i \in \mathbb{H}^*$ is written with only one subscript, as $R_i \in SO(3)$.

Algorithm 1 (Kinematic Propagation)**.** *The algorithm is initialized with the vessel configuration $p_{00} \in \mathbb{R}^3$ and $r_0 \in \mathbb{H}^*$. Then, varying index i from 0 to $n-1$, the configuration of each frame with respect to the vessel frame $\mathbf{E}_0$ can be computed by*

$$p_{0,i+1} = p_{0,i} + R_i\, p_{i,i+1}^i , \tag{12}$$

$$\overline{r}_{i+1} = \mathbf{H}_+(r_i)\, \overline{r}_{i+1}^i , \tag{13}$$

with R_i computed from r_i in (11)*. The camera pose can be computed as $p_{0c} = p_{0n} + R_c\, p_{nc}^n$, $r_c = \mathbf{H}_+(r_n)\, \overline{r}_c^n$.*

Let $\vec{v}_i$ and $\vec{\omega}_i$ be the physical linear and angular velocities of $\mathbf{E}_i$. They are represented by $v_i^i \in \mathbb{R}^3$ and $\omega_i^i \in \mathbb{R}^3$ when written in its own body frame. Let $r_i = \{\eta_i, \epsilon_i\} \in \mathbb{H}^*$ be the absolute rotation of $\mathbf{E}_i$. The time-derivative of r_i can be related to ω_i^i by

$$\dot{\overline{r}}_i = \begin{bmatrix} \dot{\eta}_i \\ \dot{\epsilon}_i \end{bmatrix} = \frac{1}{2}\, \mathbf{h}_+(r_i)\, \omega_i^i , \tag{14}$$

which is known as the *quaternion propagation* formula [15].

The vector $V_i^i = [\,(v_i^i)^\mathsf{T}\ (\omega_i^i)^\mathsf{T}\,]^\mathsf{T} \in \mathbb{R}^6$ is the *body velocity twist* associated to $\mathbf{E}_i$. Two body velocity twists associated to different frames $\mathbf{E}_i$, $\mathbf{E}_j$ located in the *same rigid-body* are related through the constant adjoint map $Ad_{g_{ij}} \in \mathbb{R}^{6\times 6}$:

$$V_i^i = Ad_{g_{ij}} V_j^j , \quad Ad_{g_{ij}} = \begin{bmatrix} R_{ij} & \hat{p}_{ij}^i R_{ij} \\ 0 & R_{ij} \end{bmatrix} , \tag{15}$$

which has the property $Ad_{g_{ji}} = Ad_{g_{ij}}^{-1}$.

Now, given the body twists V_0^0 and $\dot{V}_0^0$ of frame $\mathbf{E}_0$ in the ship, it is possible to compute all velocities V_i^i and accelerations $\dot{V}_i^i$ associated to each link ($i = 1, 2, 3$) by means of an iterative algorithm described below. It consists in propagating the body velocity/acceleration twists of each link frame $\mathbf{E}_i$ through the system, obtaining V_i^i, $\dot{V}_i^i$, $i \in \{1, 2, 3\}$.

Algorithm 2 (Propagation of Velocities and Accelerations)**.** *The algorithm is initialized with given V_0^0, $\dot{V}_0^0$. Then, the velocities and accelerations are propagated upwards the kinematic chain from $i = 0$ until $i = n = 3$:*

$$V_i^i = \Omega_{i-1,i}^\mathsf{T}\, (\Phi_{i,i-1}\, V_{i-1}^{i-1} + H_i\, \dot{q}_i) , \tag{16}$$

$$\dot{V}_i^i = \Omega_{i-1,i}^\mathsf{T}\, (\Phi_{i,i-1}\, \dot{V}_{i-1}^{i-1} + H_i\, \ddot{q}_i + A_i\, \dot{q}_i) . \tag{17}$$

The velocity/acceleration twists of the camera are computed by $V_c^c = Ad_{g_{cn}} V_n^n$, $\dot{V}_c^c = Ad_{g_{cn}} \dot{V}_n^n$, with a constant transformation g_{cn}. The matrices in (16)*,* (17) *are given by*

$$\Phi_{i+1,i} = \begin{bmatrix} \mathbf{I}_3 & -\mathbf{S}(p_{i,i+1}^i) \\ 0 & \mathbf{I}_3 \end{bmatrix} , \qquad \Phi_{i+1,i}^{-1} = \begin{bmatrix} \mathbf{I}_3 & \mathbf{S}(p_{i,i+1}^i) \\ 0 & \mathbf{I}_3 \end{bmatrix} ,$$

$$H_{i+1}^\mathsf{T} = \begin{bmatrix} 0^\mathsf{T}\ (h_{i+1}^i)^\mathsf{T} \end{bmatrix} , \qquad \Omega_{i,i+1} = \begin{bmatrix} R_{i,i+1} & 0 \\ 0 & R_{i,i+1} \end{bmatrix} ,$$

$$A_{i+1} = \begin{bmatrix} \mathbf{S}(v_i^i + \mathbf{S}(\omega_i^i)\, p_{i,i+1}^i)\, h_{i+1}^i \\ \mathbf{S}(\omega_i^i)\, h_{i+1}^i \end{bmatrix}$$

where the rotation matrices $R_{i,i+1}$ are computed from $r_{i,i+1} = \left\{cos\left(\frac{1}{2} q_{i+1}\right), h_{i+1}^i\, sin\left(\frac{1}{2} q_{i+1}\right)\right\} \in \mathbb{H}^*$ using (11)*.*

Now, recall that ω_i^i can be written as the sum $\omega_i^i = \omega_0^i + \omega_{0,i}^i$ and can be expressed in terms of $q\,, \dot{q} \in \mathbb{R}^3$ by means of the *angular body link Jacobian* $J_{0i}^i(q, \Pi_g) \in \mathbb{R}^{3\times 3}$ as $\omega_{0,i}^i = J_{0i}^i(q, \Pi_g)\, \dot{q}$:

$$\omega_i^i = J_{0i}^i(q, \Pi_g)\, \dot{q} + \omega_0^i , \tag{18}$$

where Π_g is the vector of *geometric* parameters of the ISP, containing combinations of components of the axes and distance vectors of each link frame. Note that the body link Jacobian $J_{0i}^i(q, \Pi_g)$ can be computed numerically from (16) by initializing the algorithm with $V_0^0 = 0$ and propagating three times using $q_i = [\,1\ 0\ 0\,]^\mathsf{T}$, $q_i = [\,0\ 1\ 0\,]^\mathsf{T}$ and $q_i = [\,0\ 0\ 1\,]^\mathsf{T}$ to compute each column of J_{0i}^i.

These kinematic relations can be used to describe the dependance among vehicle, ISP and camera motion by applying the group operation of $\mathbb{H}^*$, equation (18) and its time-derivative, with $\mathbf{E}_i = \mathbf{E}_c$, yielding

$$r_c = r_0 \circ r_c^0(q, \Pi_g) , \tag{19}$$

$$\omega_c^c = J_{0c}^c(q, \Pi_g)\, \dot{q} + \omega_0^c , \tag{20}$$

$$\dot{\omega}_c^c = J_{0c}^c(q, \Pi_g)\, \ddot{q} + \dot{J}_{0c}^c(q, \dot{q}, \Pi_g)\, \dot{q} + \dot{\omega}_0^c . \tag{21}$$

An important algebraic property is the *linearity* of (20) with respect to the *geometric* parameters [16]:

$$\omega_c^c = W_\omega(q, \dot{q}, \omega_0^c)\, \Pi_g . \tag{22}$$

where $W_\omega \in \mathbb{R}^{3\times N_g}$ is a *kinematic regressor*.

C. Dynamic Equations for Vehicle Manipulator Systems

In [17], it is shown that the equations of motion for a VMS with respect to the vehicle frame $\mathbf{E}_0$ can be written as:

$$M_{qq}\, \ddot{q} + C_{qq}\, \dot{q} + G_q + M_{qV}\, \dot{V}_0^0 + C_{qV}\, V_0^0 = \tau_q , \tag{23}$$

where $\tau_q \in \mathbb{R}^n$ is the vector of generalized forces acting on the robot joints, collocated with $\dot{q}$. Matrices $M_{qq}(q, \Pi_g, \Pi_d) \in \mathbb{R}^{3\times 3}$ and $M_{qV}(q, \Pi_g, \Pi_d) \in \mathbb{R}^{3\times 6}$ are mass matrices, $C_{qq}(q, \dot{q}, V_0^0, \Pi_g, \Pi_d) \in \mathbb{R}^{3\times 3}$ and

$C_{qV}(q, \dot{q}, V_0^0, \Pi_g, \Pi_d) \in \mathbb{R}^{3\times 6}$ are Coriolis matrices and $G_q(q, r_0, \Pi_g, \Pi_d) \in \mathbb{R}^3$ is the gravity vector.

It is worth mentioning that, in a similar way than in (22), (23) is also *linear* with respect to the *dynamic* parameters [16]:

$$Y_q(q, \dot{q}, \ddot{q}, r_0, V_0^0, \dot{V}_0^0, g, \Pi_g)\, \Pi_d = \tau_q\,, \tag{24}$$

where $Y_q \in \mathbb{R}^{3\times N_d}$ is a *dynamic regressor*.

The *Newton Euler* method is a computationally efficient algorithm that can be used to numerically solve the *inverse dynamics* problem for (23) [16]. Given q, $\dot{q}$, $\ddot{q}$, r_0, V_0^0, $\dot{V}_0^0$ and $g \in \mathbb{R}$, the *Newton-Euler* algorithm for the inverse dynamics is expressed by

$$\tau_q = NE(q, \dot{q}, \ddot{q}, r_0, V_0^0, \dot{V}_0^0, g, \Pi)\,, \tag{25}$$

where $\Pi^\mathsf{T} = \begin{bmatrix} \Pi_g^\mathsf{T} & \Pi_d^\mathsf{T} \end{bmatrix}$ contains combinations of the geometric and dynamic parameters (masses and inertias).

The Newton-Euler algorithm is composed of two steps. The first one is the *propagation of velocities and accelerations* upwards the kinematic chain, summarized in Algorithm 2. The second one consists in solving the dynamic equations of motion for each rigid body in the system, starting from the n-th link and ending up on $\mathbf{E}_0$.

Algorithm 3 (Backward Propagation of Wrenches)**.** *Solving the Newton-Euler equations for the contact body wrenches $F_i^i \in \mathbb{R}^6$ between the VMS bodies (links and vehicle), yields:*

$$\begin{aligned} F_i^i &= \Phi_{i+1,i}^\mathsf{T}\, \Omega_{i,i+1}\, F_{i+1}^{i+1} + M_i\, \dot{V}_i^i + B_i\,, \\ M_i &= \begin{bmatrix} m_i\, \mathbf{I}_3 & -m_i\, \mathbf{S}(p_{i\bar{i}}^i) \\ m_i\, \mathbf{S}(p_{i\bar{i}}^i) & I_i^i \end{bmatrix}, \\ B_i &= \begin{bmatrix} m_i\, \mathbf{S}(\omega_i^i)\, (\mathbf{S}(\omega_i^i)\, p_{i\bar{i}}^i + v_i^i) \\ m_i\, \mathbf{S}(p_{i\bar{i}}^i)\, \mathbf{S}(\omega_i^i)\, v_i^i + \mathbf{S}(\omega_i^i)\, I_i^i\, \omega_i^i \end{bmatrix}, \end{aligned} \tag{26}$$

where the parameters $p_{i\bar{i}}^i$, m_i and I_i^i compose Π_d in (25)*.*

These equations must be solved from $i = n = 3$ to $i = 1$, using the velocity and acceleration twists V_i^i and $\dot{V}_i^i$ previously computed in Algorithm 2. Also, we set here $n+1 = c$ and we do not consider external wrenches acting on the camera frame $\mathbf{E}_c$, so that $F_{n+1}^{n+1} = 0$.

Finally, the joint torques can be computed projecting the wrenches acting on frames $\mathbf{E}_i$ into their rotation axis by:

$$\tau_{q_i} = H_i^\mathsf{T}\, \Omega_{i-1,i}\, F_i^i\,. \qquad i = 1, ..., n\,. \tag{27}$$

Note that (26) does not take into account the gravity forces acting on the links. The effect of gravity (in $-z_0$ direction) is introduced by modifying $\dot{V}_i^i$ in (26) for each i-th link with:

$$\dot{V}_i^i \leftarrow \dot{V}_i^i - g \begin{bmatrix} R_i^\mathsf{T}\, z_0 \\ 0 \end{bmatrix}. \tag{28}$$

This algorithm can be used to compute the terms and some matrices of (23) separately: the mass matrices M_{qq}, M_{qV}, the gravity vector G_q and the Coriolis term $C_{qq}\, \dot{q} + C_{qV}\, V_0^0$.

III. Super-Twisting Control with Quaternion Feedback

In this section, a novel second-order sliding mode (SOSM) controller based on super-twisting algorithm (STA) will be developed for the stabilization and tracking of the ISP. Two cases are considered: STC with full state feedback and STC with output feedback.

Consider (23), rewritten here as:

$$M_{qq}\, \ddot{q} + \tau_d = \tau_q\,, \tag{29}$$

where $\tau_q \in \mathbb{R}^3$ is the vector of generalized forces acting on the robot joints, collocated with $\dot{q}$ and $\tau_d = C_{qq}\, \dot{q} + G_q + M_{qV}\, \dot{V}_0^0 + C_{qV}\, V_0^0 \in \mathbb{R}^3$ is a disturbance vector. The dynamic model (29) can be rewritten as:

$$\begin{aligned} \dot{x}_1 &= x_2\,, \\ \dot{x}_2 &= M_{qq}^{-1}(x_1, \Pi)\, \tau_q + x_3(x_1, x_2, \Pi, t)\,, \end{aligned} \tag{30}$$

where the states $x_1 = q$, $x_2 = \dot{q}$ are the ISP joint angles and velocities and $x_3 = -M_{qq}^{-1}(x_1)\, \tau_d$ is a state-dependent disturbance.

Remark 2. *Note that, under assumption of torque control $u(t) = \tau_q$, state-space model* (30) *is a double-integrator with a nonlinear high-frequency gain and a matched disturbance $x_3 \in \mathbb{R}^3$.*

Now, in a similar way than in (30), (14) and (21) can be rewritten as:

$$\begin{aligned} \dot{y}_1 &= \frac{1}{2}\, \mathbf{h}_+(y_1)\, y_2\,, \\ \dot{y}_2 &= J_{0c}^c(x_1, \Pi_g)\, \dot{x}_2 + y_3(x_1, x_2, \Pi_g, t)\,. \end{aligned} \tag{31}$$

where the state $y_1^\mathsf{T} = \bar{r}_c^\mathsf{T} = \begin{bmatrix} y_{11} & y_{12}^\mathsf{T} \end{bmatrix}$ is the vector representation of the camera orientation $r_c \in \mathbb{H}^*$, with $y_{11} = \eta_c$ and $y_{12} = \epsilon_c$ being the scalar and vector components. State $y_2 = \omega_c^c$ is the camera angular velocity, while $y_3 = \dot{J}_{0c}^c\, \dot{q} + \dot{\omega}_0^c$ is another state-dependent disturbance.

Remark 3. *Note that the state-space model* (31) *is a double integrator with a nonlinear high-frequency gain and a matched disturbance y_3 with respect to a control input $\dot{x}_2$.*

This structure strongly suggests the use of a *cascade controller* for both stabilization and tracking. An inner controller acts on $u(t)$ in (30) to control $\dot{x}_2$, providing dynamic stabilization for the system, while an outer tracking controller acts on $\dot{x}_2$ in (31), controlling the camera orientation y_1.

Given an orientation reference $r_{c_d}(t) \in \mathbb{H}^*$ for the camera, it can be represented in vector form by $\bar{r}_{c_d}^\mathsf{T}(t) = y_{1_d}^\mathsf{T}(t) = \begin{bmatrix} y_{11_d}(t) & y_{12_d}^\mathsf{T}(t) \end{bmatrix}$. The angular velocity of the camera is also given as $\omega_{c_d}^c(t) = y_{2_d}(t)$. The quaternion and angular velocity errors can be defined as:

$$e_c = r_{c_d}(t) \cdot r_c^*\,, \tag{32}$$

$$e_\omega = y_{2_d}(t) - y_2\,. \tag{33}$$

Note that when $r_c = r_{c_d}(t)$, the orientation error (32) is zero.

A. Super-Twisting Control with Full State Feedback

Suppose that both ISP states x_1 and x_2 are available. The following theorem provides an stability analysis for the proposed sliding mode cascade controller.

Theorem 1 (*Cascade STC with Full State Feedback*)**.** *Let* (30) *and* (31) *be the system dynamic and kinematic models. Assume the following:*

(i) the ISP joint velocities and accelerations are uniformly norm-bounded;

(ii) the zero, first and second order time-derivatives of the vehicle velocity twists are uniformly norm-bounded;

Defining the super-twisting control expression

$$S_t(s, A, B) = A\lfloor s \rceil^{1/2} + B \int_0^t sgn(s) d\tau \,,$$

with matrices $A, B > 0$, the super-twisting-based controllers can be defined as follows. The outer sliding surface is

$$s_y = e_\omega + K_c \, \mathsf{lm}(e_c) \,, \quad K_c > 0 \,, \tag{34}$$

where $K_c > 0$. The corresponding outer control law is

$$w(t) = \widehat{J}_{0c}^{c}(x_1)^{-1} \left[\dot{y}_{2_d}(t) + K_c \, \psi + S_t(s_y, \Lambda_3, \Lambda_4) \right] . \tag{35}$$

where $\widehat{J}_{0c}^{c}(x_1) = J_{0c}^{c}(x_1, \widehat{\Pi}_g)$ and ψ is a function of y_1, y_2 and r_{c_d}. The inner sliding surface is defined as

$$s_x = x_2 - \int_0^t w(\tau) \, d\tau \,, \tag{36}$$

and the corresponding inner control law is

$$u(t) = \widehat{M}_{qq}(x_1) \, \left[w(t) - S_t(s_x, \Lambda_1, \Lambda_2) \right] , \tag{37}$$

where $\widehat{M}_{qq}(x_1) = M_{qq}(x_1, \widehat{\Pi}_g, \widehat{\Pi}_d)$. Then, control laws (37) *and* (35) *ensure finite-time exact convergence of the sliding variables s_x and s_y as defined in* (36) *and* (34)*. Furthermore, the quaternion and angular velocity errors e_c, e_ω are asymptotically stable under the dynamics of $s_y = 0$.*

Proof. Using (30) and Assumption 3, the dynamics of the sliding variable s_x is given by:

$$\dot{s}_x = \dot{x}_2 - w(t) = M_{qq}^{-1} \, u(t) + x_3 - w(t) \,. \tag{38}$$

Substituting (37) into (38), it becomes:

$$\dot{s}_x = -(\mathbf{I}_3 - M_{qq}^{-1} \, \Delta M_{qq}) \, S_t(s_x, \Lambda_1, \Lambda_2) + x_3 \,, \tag{39}$$

where $\Delta M_{qq} = M_{qq} - \widehat{M}_{qq}$. Using (24), $\Delta M_{qq} \, S_t = Y_q^* \, \widetilde{\Pi}_d + \Delta Y_q^* \, \widehat{\Pi}_d$, with $\Delta Y_q^* = Y_q^* - \widehat{Y}_q^*$, where $Y_q^* = Y_q(x_1, 0, S_t(s_x, \Lambda_1, \Lambda_2), 0, 0, 0, 0, \Pi_g)$ and $\widehat{Y}_q^* = Y_q(x_1, 0, S_t(s_x, \Lambda_1, \Lambda_2), 0, 0, 0, 0, \widehat{\Pi}_g)$. Then, it is possible to rewrite (39) as:

$$\begin{aligned} \dot{s}_x &= -\Lambda_1 \lfloor s_x \rceil^{1/2} + w_x \,, \\ \dot{w}_x &= -\Lambda_2 \lfloor s_x \rceil^{0} + d_x \,, \end{aligned} \tag{40}$$

where $d_x = \nabla(M_{qq}^{-1} \, Y_q^*) \, \widetilde{\Pi}_d + \nabla(M_{qq}^{-1} \, \Delta Y_q^*) \, \widehat{\Pi}_d + \dot{x}_3$ is clearly dependent on the base motion and on the errors on the geometric and dynamic parameters. Here, the operator ∇ denotes time differentiation.

Note that (40) is STA, and therefore is finite-time stable for bounded disturbances. It is evident that, if the nominal parameters are well known, system (39) is only perturbed by $d_x \approx \dot{x}_3$. Due to Assumptions (i) and (ii), the following inequalities hold:

$$\left\| \nabla(M_{qq}^{-1} \, Y_q^*) \, \widetilde{\Pi}_d \right\| < L_{x_1} \,, \tag{41}$$

$$\left\| \nabla(M_{qq}^{-1} \, \Delta Y_q^*) \, \widehat{\Pi}_d \right\| < L_{x_2} \,, \tag{42}$$

$$\| \dot{x}_3 \| < L_{x_3} \,. \tag{43}$$

Then, $\| d_x \| < L_{x_1} + L_{x_2} + L_{x_3}$, and according to [18], it is possible to chose Λ_1 and Λ_2 so that (40) achieves SOSM in finite-time. It means that after a time $T_1 > 0$, $s_x = \dot{s}_x = 0$ and due to (38), $\dot{x}_2 = w(t) \; \forall t > T_1$, even in the presence of the bounded disturbance d_x.

Next, using (31), (32) and (33), the dynamics of the outer sliding variable (34) is given by

$$\dot{s}_y = \dot{y}_{2_d} - J_{0c}^{c}(x_1) \, \dot{x}_2 - y_3 + K_c \, \psi \,, \tag{44}$$

where $\psi(y_1, y_2, r_{c_d}) = y_{11} \, \dot{y}_{12_d} - 0.5 \, y_{12}^{\mathsf{T}} \, y_2 \, y_{12_d} - \dot{y}_{11_d} \, y_{12} - \dot{\widehat{y}}_{12_d} \, y_{12} - 0.5 \, y_{11_d} \, (y_{11} \, \mathbf{I}_3 - \widehat{y}_{12}) \, y_2 - 0.5 \, \widehat{y}_{12_d} \, (y_{11} \, \mathbf{I}_3 - \widehat{y}_{12}) \, y_2$, with $\dot{y}_{1_d} = \mathbf{h}_-(y_1) \, y_{2_d}$.

Since $\dot{x}_2 = \dot{s}_x + w(t)$, substituting (35) into (44) yields:

$$\begin{aligned} \dot{s}_y &= -\Lambda_3 \lfloor s_y \rceil^{1/2} + w_y \,, \\ \dot{w}_y &= -\Lambda_4 \lfloor s_y \rceil^{0} + d_y \,, \end{aligned} \tag{45}$$

where $d_y = -\dot{y}_3 - \nabla(J_{0c}^{c} \, \dot{s}_x) - \nabla(W_\omega^*) \widetilde{\Pi}_g$, with $W_\omega^* = W_\omega(x_1, w(t), 0)$, according to (22). Again, due to Assumptions (i) and (ii):

$$\| \nabla(J_{0c}^{c} \, \dot{s}_x) \| < L_{y_1} \,, \tag{46}$$

$$\left\| \nabla(W_\omega^*) \widetilde{\Pi}_g \right\| < L_{y_2} \,, \tag{47}$$

$$\| \dot{y}_3 \| < L_{y_3} \,. \tag{48}$$

Note that (46) is reasonable, since $\ddot{s}_x$ is bounded, but constant L_{y_1} clearly depends on the initial conditions of (30). Also, in (47), $\nabla(W_\omega^*)$ depends on x_1, x_2, $w(t)$ and $\dot{w}(t)$, which are also bounded. Then, $\| d_y \| < L_{y_1} + L_{y_2} + L_{y_3}$, again guaranteeing finite-time stabilization of (45) after a time $T_2 > 0$. It means that for all $t \geq T_2$, the system is sliding and therefore, it follows the nonlinear dynamics of the sliding variable (34), which is asymptotically stable [16]. Therefore, the quaternion errors (32) and (33) tend to zero asymptotically after a time $max(T_1, T_2)$.

□

B. Super-Twisting Control with HOSM Observer

If state $x_2 \in \mathbb{R}^3$ is not available, an observer could be used to estimate the joint velocity state $x_2(t)$ using the measurements of $x_1(t)$. Because of its desired characteristics such as finite-time exact convergence, sliding mode observers

could be used for this purpose, such as the *super-twisting* observer (STO) [18]. However, according to [19], it is not possible to achieve *second order sliding* ($s = \dot{s} = 0$) using *continuous* control when STC is implemented based on ST observers. A proposed solution is to use STC with HOSM-based observers to achieve continuous control.

Remark 4. *Two HOSMOs could be designed: one for the joint velocities $x_2(t)$, and other for the camera angular velocity $y_2(t)$. However, usually the camera orientation $y_1(t)$ is obtained from an Inertial Measurement Unit (IMU), a device that combines measurements of gyroscopes (which measure angular velocity) and magnetometers (which measure magnetic fields), providing an accurate estimate for $y_1(t)$. Therefore, trustworthy direct measurements of $y_2(t)$ are usually already available.*

Theorem 2 (*Cascade STC with Output Feedback*)**.** *Let* (30) *and* (31) *be the system dynamic and kinematic models. Assume the following:*

(i) the ISP joint velocities and accelerations are uniformly norm-bounded;

(ii) the zero, first and second order time-derivatives of the vehicle velocity twists are uniformly norm-bounded;

Defining the estimation error $e_{x_1} = x_1 - \hat{x}_1$, the HOSM observer for x_2 is the third-order system:

$$\begin{aligned}\dot{\widehat{x}}_1 &= K_1 \lfloor e_{x_1} \rceil^{2/3} + \widehat{x}_2 \,,\\ \dot{\widehat{x}}_2 &= K_2 \lfloor e_{x_1} \rceil^{1/3} + \widehat{x}_3 + \widehat{M}_{qq}^{-1}(x_1)\, u \,,\\ \dot{\widehat{x}}_3 &= K_3 \lfloor e_{x_1} \rceil^{0} \,. \end{aligned} \tag{49}$$

where K_1, K_2 and K_3 are positive-definite matrices. The outer sliding variable and control law are defined in the same way as (34) *and* (35)*. The modified inner sliding variable is:*

$$\widehat{s}_x = \widehat{x}_2 - \int_0^t w(\tau)\, d\tau \,, \tag{50}$$

and the corresponding inner control law is:

$$u(t) = \widehat{M}_{qq}(x_1) \left[w(t) - K_2 \lfloor e_{x_1} \rceil^{1/3} - S_t(\widehat{s}_x, \Lambda_1, \Lambda_2) \right] . \tag{51}$$

Then, control laws (51) *and* (35) *with observer* (49) *ensure finite-time exact convergence of the sliding variables s_x and s_y as defined in* (50) *and* (34)*, and of the estimation errors e_{x_1}, $e_{x_2} = x_2 - \widehat{x}_2$ and $e_{x_3} = x_3 - \widehat{x}_3$. Furthermore, the quaternion and angular velocity errors e_c, e_ω are asymptotically stable under the dynamics of $s_y = 0$.*

Proof. Using (30) and (49), the dynamics of the estimation errors is:

$$\begin{aligned}\dot{e}_{x_1} &= -K_1 \lfloor e_{x_1} \rceil^{2/3} + e_{x_2} \,,\\ \dot{e}_{x_2} &= -K_2 \lfloor e_{x_1} \rceil^{1/3} + e_{x_3} + (M_{qq}^{-1} - \widehat{M}_{qq}^{-1})\, u \,,\\ \dot{e}_{x_3} &= -K_3 \lfloor e_{x_1} \rceil^{0} + \dot{x}_3 \,. \end{aligned} \tag{52}$$

By using transformation $e_{x_4} = e_{x_3} + (M_{qq}^{-1} - \widehat{M}_{qq}^{-1})\, u$, it is possible to rewrite (52) as:

$$\begin{aligned}\dot{e}_{x_1} &= -K_1 \lfloor e_{x_1} \rceil^{2/3} + e_{x_2} \,,\\ \dot{e}_{x_2} &= -K_2 \lfloor e_{x_1} \rceil^{1/3} + e_{x_4} \,,\\ \dot{e}_{x_4} &= -K_3 \lfloor e_{x_1} \rceil^{0} + d_e \,. \end{aligned} \tag{53}$$

where $d_e = \dot{x}_3 + (M_{qq}^{-1} - \widehat{M}_{qq}^{-1})\, \dot{u} + \nabla(M_{qq}^{-1} - \widehat{M}_{qq}^{-1})\, u$. Due to Assumption (i) and (51), two constants $L_{e_1}, L_{e_2} > 0$ exist, such that:

$$\left\| (M_{qq}^{-1} - \widehat{M}_{qq}^{-1})\, \dot{u} \right\| < L_{e_1} \,, \tag{54}$$

$$\left\| \nabla(M_{qq}^{-1} - \widehat{M}_{qq}^{-1})\, u \right\| < L_{e_2} \,. \tag{55}$$

Also, by Assumption (ii), $\|\dot{x}_3\| < L_{x_3}$ also holds. Then, $\|d_e\| < L_{e_1} + L_{e_2} + L_{x_3}$, and therefore the disturbance d_e is norm-bounded. According to [20], it is possible to chose K_1, K_2 and K_3 so that the states on (53) are finite-time stable.

Remark 5. *Since $M_{qq}^{-1} - \widehat{M}_{qq}^{-1} \neq 0$ due to parametric uncertainty, the estimation error e_{x_3} is expected to be norm-bounded only. Therefore, $x_3 = \widehat{x}_3 + \beta(\widetilde{\Pi})$, where $\beta(\widetilde{\Pi})$ is a small residue dependent on the parametric uncertainty.*

The dynamics of the modified sliding variable is given by:

$$\dot{\widehat{s}}_x = K_2 \lfloor e_{x_1} \rceil^{1/3} + \widehat{x}_3 + \widehat{M}_{qq}^{-1}(x_1)\, u(t) - w(t) \,. \tag{56}$$

Using the *continuous* control law (51), yields:

$$\begin{aligned}\dot{\widehat{s}}_x &= -\Lambda_1 \lfloor \widehat{s}_x \rceil^{1/2} + \widehat{w}_x \,,\\ \dot{\widehat{w}}_x &= -\Lambda_2 \lfloor \widehat{s}_x \rceil^{0} + K_3 \lfloor e_{x_1} \rceil^{0} \,. \end{aligned} \tag{57}$$

Since the disturbance $K_3 \lfloor e_{x_1} \rceil^0$ is obviously norm-bounded, the STA (57) is finite-time stable. Therefore, after a finite time $\bar{T}_1 > 0$, $\dot{x}_2 = w(t)$.

To prove the stability of the outer controller, a similar procedure is performed. Since $\dot{x}_2 = \dot{\widehat{s}}_x + \dot{e}_{x_2} + w(t)$, substituting (35) into (44) yields:

$$\begin{aligned}\dot{s}_y &= -\Lambda_3 \lfloor s_y \rceil^{1/2} + w_y \,,\\ \dot{w}_y &= -\Lambda_4 \lfloor s_y \rceil^{0} + \bar{d}_y \,, \end{aligned} \tag{58}$$

where $\bar{d}_y = -\dot{y}_3 - \nabla(J_{0c}^c\, \dot{\widehat{s}}_x) + \nabla(J_{0c}^c \dot{e}_{x_2}) - \nabla(W_\omega^*)\widetilde{\Pi}_g$. Again, due to Assumptions (i) and (ii), (53) and (57), two positive constants $\bar{L}_{y_1}$, $\bar{L}_{y_2}$ exist, such that:

$$\left\| \nabla(J_{0c}^c\, \dot{\widehat{s}}_x) \right\| < \bar{L}_{y_1} \,, \tag{59}$$

$$\| \nabla(J_{0c}^c \dot{e}_{x_2}) \| < \bar{L}_{y_2} \,, \tag{60}$$

Then, $\left\|\bar{d}_y\right\| < \bar{L}_{y_1} + \bar{L}_{y_2} + L_{y_2} + L_{y_3}$, again guaranteeing finite-time stabilization of (58) after a time $\bar{T}_2 > 0$. Therefore, the quaternion errors (32) and (33) tend to zero asymptotically after a time $max(\bar{T}_1, \bar{T}_2)$.

□

IV. Simulation Results

This section presents the results of the proposed control methods. MATLAB Simulink® models were implemented for the simulation of the dynamic model of a 3-DOF ISP installed on a vessel and for the implementation of the cascade Super Twisting Control (STC) strategies proposed in Section III.

Joint friction torques were simulated as the sum of Stribeck, Coulomb and viscous friction components, and a saturation of $\pm 12.2\, Nm$ in each joint motor was considered. The joint encoders and the INS were modeled considering hardware effects such as resolution, bias and noise, and the base motion data were obtained from the simulation of a vessel subject to Jonswap spectrum waves with 200 harmonics, 3m height, 10s time period, and acting on the longitudinal axis of the vessel.

Remark 6. *The presented control methods can be applied to any kind of vehicle or moving base where the ISP is installed, since the quaternion formalism does not suffer from representation singularities and the base dynamics (velocities and accelerations) only affect the overall magnitude of the gains.*

TABLE I
KINEMATIC AND DYNAMIC MODEL PARAMETERS, IN SI UNITS.

Parameter	$i=1$			$i=2$			$i=3$		
	x	y	z	x	y	z	x	y	z
$p^{i}_{i\bar{i}}$	0.006	0.023	0.326	-0.094	0.006	0.059	0.336	0.006	-0.023
$p^{i-1}_{i-1,i}$	0.3	0	0	0	0	0.436	-0.254	0	0
$I^{\bar{i}}_{i}$	2.42	0.58	1.93	1.12	0.92	0.88	0.54	0.93	0.86
m_i	18.9			21			26.5		

Table I contains the kinematic and dynamic parameters used in the simulations. The *real* joint axis are considered as $h^0_1 = z_0$, $h^1_2 = y_0$ and $h^2_3 = x_0$. Also, we have $p^3_{3c} = \begin{bmatrix} 0.555 & 0 & 0.014 \end{bmatrix}^{\mathsf{T}}$, and the inertia tensor represented in $\mathbf{E}_i$ can be computed from the *Huygens-Steiner theorem* as $I^i_i = I^{\bar{i}}_{\bar{i}} - m_i\,(\widehat{p}^i_{i\bar{i}})^2$. These parameters were obtained from the mechanical design of a 3-DOF ISP currently being developed by a collaboration among several groups, including the authors laboratory (LEAD/COPPE/UFRJ).

The mass matrices in (37) and (51) and the Jacobian matrix in (35) were computed using numerical algorithms, implemented with MATLAB® mex files. The values for the nominal parameters used in control were set as the real values in Table I with a percentage of error. The gains for both state and output feedback controllers were set as $\Lambda_1 = \Lambda_2 = 10\,\mathbf{I}_3$, $\Lambda_3 = \Lambda_4 = 15\,\mathbf{I}_3$, and the HOSMO gains were chosen as $K_1 = K_2 = K_3 = 15$. These values are sufficient to overcome the magnitude of the disturbances and small enough to avoid chattering effects. The quaternion reference was computed from the roll $\phi_c(t)$, pitch $\theta_c(t)$ and yaw $\psi_c(t)$ (RPY) references for the camera orientation $\eta_c(t) = [\,\phi_c(t)\ \theta_c(t)\ \psi_c(t)\,]^{\mathbf{T}}$, consisting of unbiased sines with 60° of amplitude and $10\,s$ period.

A. Full State Feedback STC

Figure 1 shows the transient and steady-state response of the state feedback STC in terms of RPY errors for the case of 50% of parametric error and 5° degrees of axis misalignment in the computation of the Jacobian matrix. Both stabilization

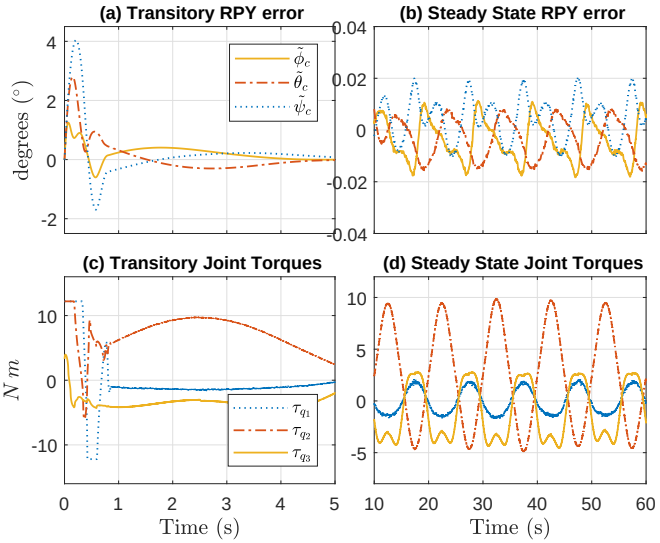

Fig. 1. Response for state feedback STC controller with 50% of parametric error and 5° degrees of axis misalignment.

and tracking controllers achieve SOSM in less than $2\,s$, with sliding accuracy on s_x and s_y approximately equal to $10^{-4}\,rad/s$ and 10^{-5}, respectively. The RPY jitter converges to a small region of 0.02° in approximately $10\,s$ due to the chosen dynamics for the outer sliding surface.

B. Output Feedback STC + HOSMO

Figure 2 shows the transient and steady-state response of the of the output feedback STC, in the same conditions as before. The transient and performance remains practically

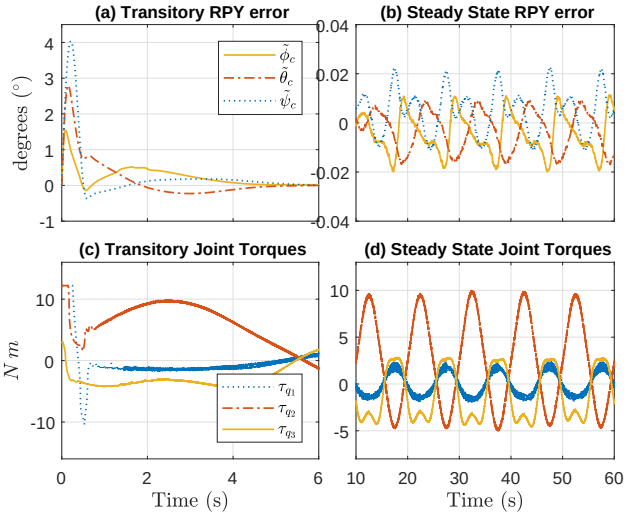

Fig. 2. Response for output feedback STC controller with 50% of parametric error and 5° degrees of axis misalignment.

the same, with a very small increase in the RPY jitter and in the control chattering. This is due to the presence of the term dependent multiplying K_2 in (51).

Figure 3 shows the HOSMO estimation errors of the output feedback STC scheme. Note that finite-time convergence

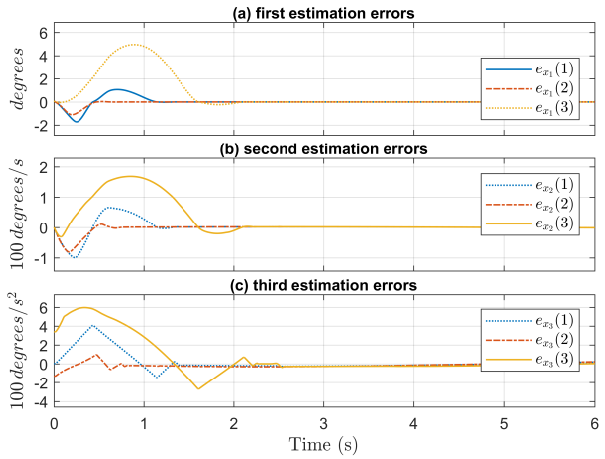

Fig. 3. HOSMO estimation errors for output feedback STC controller with 50% of parametric error.

is achieved in approximately $3\,s$, even in the presence of sensor noise and 50% of parametric error in $\widehat{M}_{qq}$ used in (49).

V. Conclusion and Future Works

In this work, we have proposed a cascade super-twisting control (STC) method for stabilization and tracking of a 3-DOF ISP. Both full state and output feedback cases are considered; the further employs a HOSM observer for joint velocity estimation. Although the algorithms use the ISP mass matrix and its geometrical Jacobian, the obtained tracking accuracy is much better than with P-PI or computed torque control [12], even in the presence of strong parametric uncertainty and sensor noise. Besides, considering the amplitude and frequency of the control chattering, it is reasonable to conclude that this scheme could be implemented in a real system.

In the general, the performance of the output feedback STC is very close to the full state feedback STC, but with the clear advantage of avoiding taking joint velocity measurements, which are often very noisy or obtained by other estimation methods.

Future works include a more detailed study of the analytical properties of the proposed controllers, such as the computation of the approximate convergence times and robustness to unmodeled dynamics.

VI. Acknowledgements

The authors would like to thank Tecgraf Institute of Technical and Scientific Software Development from PUC-Rio university, in Brazil, for providing the vessel motion data used in the simulations.

References

[1] Z. Hurák and M. Řezáč, "Combined line-of-sight inertial stabilization and visual tracking: application to an airborne camera platform," in *Proceedings of the IEEE Conference on Decision and Control.*, 2009, pp. 8458–8463.

[2] J. Debruin, "Control systems for mobile satcom antennas," *Control Systems, IEEE*, vol. 28, no. 1, pp. 86–101, 2008.

[3] A. Kazemy, S. A. Hosseini, and M. Farrokhi, "Target-based line-of-sight stabilization in periscopes," *Mediterranean Conference on Control and Automation*, 2007.

[4] H. Skjelten, C. Gutvik, and L. Solberg, "Ship based oil spill monitoring: A new integrated system for thickness evaluation and operational overview," in *International Oil Spill Conference Proceedings (IOSC)*, vol. 2011, no. 1. American Petroleum Institute, 2011.

[5] P. J. Kennedy and R. L. Kennedy, "Direct versus indirect line of sight (LOS) stabilization," *IEEE Transactions on Control Systems Technology*, vol. 11, no. 1, pp. 3–15, 2003.

[6] J. M. Hilkert, "Inertially stabilized platform technology: Concepts and principles," *IEEE Control Systems Magazine*, vol. 28, no. 1, pp. 26–46, 2008.

[7] M. K. Masten, "Inertially stabilized platforms for optical imaging systems," *IEEE Control Systems Magazine*, vol. 28, no. 1, pp. 47–64, 2008.

[8] P. J. Kennedy and R. Kennedy, *Stabilizing the Line of Sight*, 2014.

[9] M. Abdo, A. R. Vali, A. Toloei, and M. R. Arvan, "Research on the cross-coupling of a two axes gimbal system with dynamic unbalance," *International Journal of Advanced Robotic Systems*, vol. 10, 2013.

[10] M. M. Abdo, A. R. Vali, A. R. Toloei, and M. R. Arvan, "Stabilization loop of a two axes gimbal system using self-tuning pid type fuzzy controller," *ISA Transactions*, vol. 53, no. 2, pp. 591 – 602, 2014.

[11] F. Königseder, W. Kemmetmüller, and A. Kugi, "Attitude control strategy for a camera stabilization platform," *Mechatronics*, vol. 46, pp. 60–69, 2017.

[12] M. Reis, G. P. S. Carvalho, A. F. Neves, and A. J. Peixoto, "Dynamic model and line of sight control of a 3-dof inertial stabilization platform," in *Proceedings of the IEEE American Control Conference*, 2018.

[13] J. Mao, J. Yang, S. Li, and Q. Li, "Output feedback stabilization of inertial stabilized platform with unmatched disturbances using sliding mode approach," vol. 50, pp. 5149–5154, 07 2017.

[14] Y. Feng, X. Yu, and Z. Man, "Non-singular terminal sliding mode control of rigid manipulators," *Automatica*, vol. 38, no. 12, pp. 2159 – 2167, 2002.

[15] B. Vilhena Adorno, "Robot Kinematic Modeling and Control Based on Dual Quaternion Algebra — Part I: Fundamentals." Feb. 2017, working paper or preprint. [Online]. Available: https://hal.archives-ouvertes.fr/hal-01478225

[16] B. Siciliano, L. Sciavicco, and L. Villani, *Robotics : Modelling, Planning and Control*, ser. Advanced Textbooks in Control and Signal Processing. London: Springer, 2009, 013-81159.

[17] P. J. From, J. T. Gravdahl, and K. Y. Pettersen, *Vehicle-manipulator systems*. Springer, 2014.

[18] J. A. Moreno and M. Osorio, "Strict lyapunov functions for the super-twisting algorithm," *IEEE Transactions on Automatic Control*, vol. 57, no. 4, pp. 1035–1040, April 2012.

[19] A. Chalanga, S. Kamal, L. M. Fridman, B. Bandyopadhyay, and J. A. Moreno, "Implementation of super-twisting control: Super-twisting and higher order sliding-mode observer-based approaches," *IEEE Transactions on Industrial Electronics*, vol. 63, no. 6, pp. 3677–3685, June 2016.

[20] J. A. Moreno, "Lyapunov function for levant's second order differentiator," in *2012 IEEE 51st IEEE Conference on Decision and Control (CDC)*, Dec 2012, pp. 6448–6453.